

Original Article

# HYPOXIA-DERIVED MESENCHYMAL STEM-CELL EXOSOMES DELIVERING NARINGIN ENHANCE OSTEOBLAST MIGRATION AND FRACTURE HEALING BY UPREGULATING INTEGRIN $\beta 1$ VIA THE BDNF-TRKB/ERK1/2 SIGNALING PATHWAY

R.F. Yao<sup>1</sup>, Y.Y. Luo<sup>2</sup> and H.L. Tian<sup>3,\*</sup><sup>1</sup>Shandong University of Traditional Chinese Medicine, 250355 Jinan, Shandong, China<sup>2</sup>Department of Orthopaedics, Yantai Penglai People's Hospital, 265600 Yantai, Shandong, China<sup>3</sup>Department of Orthopaedics, Affiliated Hospital of Shandong University of Traditional Chinese Medicine, 250014 Jinan, Shandong, China

## Abstract

**Background:** The paracrine mechanism of mesenchymal stem cells (MSCs) is receiving extensive attention, and exosomes are positioned as the key mediators. MSCs subjected to hypoxic preconditioning exhibit notably enhanced paracrine functions. Recent studies have revealed that Naringin (Ng), acting through the paracrine actions of MSCs, can promote osteoblast migration and bone-fracture healing, although the detailed mechanisms behind this effect remain to be fully elucidated. This study aimed to explore the effect of hypoxia pretreatment on the bioactivity of exosomes and fracture healing through Ng regulation. **Methods:** Exosome nanoparticles containing Ng were identified by transmission electron microscopy and nanoparticle tracking analysis. *In vivo*, a fracture mice model was established by staining Ki67 CD31<sup>+</sup> and Ecmn CD31<sup>+</sup> positive cells. Bone healing after normoxia, hypoxia, normoxia + Ng, and hypoxia + Ng treatment was evaluated. *In vitro*, the effects of different interventions on human umbilical cord MSCs (HucMSCs) were evaluated experimentally by cell counting kit-8 (CCK8), 5-ethynyl-2'-deoxyuridine (EdU) staining, cell migration, Transwell invasion, and tube-formation assay. Tropomyosin receptor kinase B (TrkB), brain-derived neurotrophic factor (BDNF), and integrin  $\beta 1$ , respectively were silenced to explore the possible mechanisms promoting bone healing. **Results:** Results showed that Ng-rich exosomes significantly promoted osteoblast migration and bone healing under hypoxia conditions ( $p < 0.001$ ). Under hypoxia conditions, exosomes derived from MSCs can be used as carriers for Ng delivery. These exosomes targeted the BDNF-mediated TrkB/extracellular regulated protein kinases (ERK)1/2 signaling pathway and upregulated integrin  $\beta 1$  expression. **Conclusions:** These findings unveiled the potential mechanisms by which hypoxia-conditioned MSC-derived exosomes wrapped in Ng promoted osteoblast migration and bone-fracture healing. A theoretical foundation was also provided for using MSC-derived exosomes as a novel bone-repair treatment strategy.

**Keywords:** Mesenchymal stem cell, hypoxia, human umbilical vein endothelial cells, osteoblast migration, bone healing.

\***Address for correspondence:** H.L. Tian, Department of Orthopaedics, Affiliated Hospital of Shandong University of Traditional Chinese Medicine, 250014 Jinan, Shandong, China. Email: [tianhlai@163.com](mailto:tianhlai@163.com).

**Copyright policy:** © 2025 The Author(s). Published by Forum Multimedia Publishing, LLC. This article is distributed in accordance with Creative Commons Attribution Licence (<http://creativecommons.org/licenses/by/4.0/>).

## Introduction

Bone-fracture repair encompasses a sophisticated process that harnesses the innate regenerative capacity to reconstruct the bone's original structure while promoting the augmentation of mineralized matrices [1]. Extensive research has elucidated various critical regulatory factors integral to the osteogenesis process during bone repair [2,3]. In particular, angiogenesis has been identified as a pivotal component in bone metabolism and repair mechanisms [4]. It entails the infiltration of endothelial cells into the growth-plate cartilage, facilitating nutrient supply and forming a novel scaffold for osteogenesis. The angiogenic mecha-

nism encompasses the growth and movement of endothelial cells, the formation of capillary networks, and the stabilization of mesenchymal stem cells (MSCs) [5]. However, recent developments in fracture-management techniques have only gradually progressed.

The transplantation of MSCs shows promising therapeutic outcomes across various disease models, notably in enhancing osteogenesis and angiogenesis within stabilized fracture models [6,7]. Despite these advances, the direct transplantation of MSCs into target tissues faces significant hurdles and constraints. In ischemic tissues, transplanted stem cells exhibit markedly low survival rates [8]. Addi-

tional complications that curtail the practical application of MSC transplantation for bone-fracture repair in clinical settings include immune-system rejection, potential cell dedifferentiation, and the risk of tumorigenesis.

Recent investigations into MSCs' role in tissue regeneration suggest that their therapeutic actions may largely be mediated through paracrine effects, with exosomes playing a pivotal role in this mechanism [9,10]. Exosomes, crucial components of cell-derived paracrine signaling, form through the inward folding of endosomal membranes, resulting in multivesicular bodies that range from 50 nm to 150 nm in diameter [11–13]. These vesicles are released into the extracellular milieu by merging with the plasma membrane, thereby safeguarding their cargo from enzymatic breakdown [11,12]. They carry an array of biomolecules including cytokines, mRNAs, miRNAs, and proteins that facilitate critical intercellular communication through genetic-material transfer [13]. Notably, exosomes possess specific surface ligands that facilitate targeted binding and content delivery to recipient cells, thereby modulating distinct biological processes [11,12,14]. Evidence suggests that exosome transplantation mirrors the therapeutic and functional benefits observed with direct stem-cell transplants but with reduced associated risks [13]. For instance, MSC-derived exosomes promote angiogenesis in myocardial infarction models and mitigate rat hepatic ischemia-reperfusion injuries [15]. Stem-cell-derived exosomes can also enhance recovery following spinal cord injuries by reducing neuronal apoptosis and encouraging autophagy [16].

Oxygen concentration is pivotal in MSCs regulatory mechanisms, affecting their proliferation, differentiation, and self-maintenance [17]. Typically, MSCs are cultured under normoxic conditions (21 % O<sub>2</sub>) *in vitro*, a stark contrast to the lower oxygen tensions found within the body's physiological environments, where MSCs are often situated in hypoxic niches (2 %–8 % O<sub>2</sub>) [18]. A recent study on MSC-derived exosomes grown in environments that simulate peripheral arterial disease conditions (1 % O<sub>2</sub>) has shown that these exosomes contain pro-angiogenic factors, indicating their potential therapeutic application in treating ischemic conditions [19]. Additionally, research utilizing myocardial infarction models has shown that exosomes from MSCs conditioned in hypoxic environments exhibit enhanced pro-angiogenic properties, decrease cardiomyocyte apoptosis, and improve the recruitment of cardiac progenitor cells. This highlights the substantial potential of MSC-derived exosomes in promoting tissue regeneration and repair [20,21].

A recent study on exosome constituents including proteins, RNAs, and pharmacological agents aims to clarify their roles in treating various diseases [22]. Naringin (Ng), a key compound in traditional Chinese medicine, affects osteoblast and osteoclast functions [23,24]. The exact roles and mechanisms of action of Ng in hypoxia-conditioned MSC-derived exosomes for bone-fracture repair remain

unclear. Exosomal cargoes such as Ng can reportedly modulate the behaviors of target cells, introducing a new paradigm for intracellular communication [25]. Importantly, previous research has shown Ng's ability to enhance brain-derived neurotrophic factor (BDNF) and vascular endothelial growth factor (VEGF) expression in a rat spinal cord injury model [26]. BDNF is essential in controlling cell migration because it promotes the movement of young cardiac microvascular endothelial cells through the BDNF-tropomyosin receptor kinase B (TrkB)/extracellular regulated protein kinases (ERK)/integrin signaling pathway [27, 28]. The present study aimed to confirm the role of hypoxic preconditioning in enhancing exosome bioactivity through Ng regulation and its effects on bone-fracture healing. We demonstrated that exosomes derived from MSCs treated under hypoxic conditions and loaded with Ng specifically targeted the BDNF-mediated TrkB/ERK1/2 signaling pathway, leading to an upregulation of integrin  $\beta$ 1 expression. This process facilitated osteoblast migration and significantly improved bone-fracture healing. This discovery underscored the therapeutic promise of MSC-derived exosomes in bone repair and unveiled a novel mechanism of cellular interaction and tissue regeneration. Therefore, it can broaden the scope of regenerative medicine and pave the way for innovative clinical strategies.

## Materials and Methods

### Cell Culture

The human umbilical cord MSC (HucMSC) line (BFN60808923) was obtained from ATCC in Manassas, VA, USA and grown in dulbecco's modified eagle medium (DMEM) containing high levels of glucose, with an addition of 10 % fetal bovine serum (FBS; A5670701, Gibco, Life Technologies, Rockville, MD, USA) and 1 % antibiotics (penicillin/streptomycin, HY-K1006, MedChemExpress, Monmouth County, NJ, USA). The hFOB 1.19 cell line (JSY-CC1109, JSCALL, Shanghai, China) was cultured in a combined medium of DMEM and Ham's F-12 at equal parts, enriched with 15 % FBS, 1 % antibiotics (penicillin/streptomycin), and 0.3 mg/mL of the G418 antibiotic (10131027, Sigma, St. Louis, MO, USA) for specific growth conditions. After 24 h of cell culture, 10  $\mu$ mol/L Ng was added into the medium [24]. All cells were mycoplasma-free and short tandem repeat (STR) analysis revealed that they were derived from its parental cells.

### Exosome Isolation and Identification

Upon reaching 80 % confluence, HucMSCs were cultured for an additional 48 h in media containing exosome-depleted FBS, this was done under various conditions: normoxic (21 % O<sub>2</sub>), hypoxic (1 % O<sub>2</sub>), normoxic with Ng, and hypoxic with Ng. Preconditioning cells against hypoxia or normoxia. Simply culture the cells at 37 °C, 5 % CO<sub>2</sub>, 21 % O<sub>2</sub> or 1 % O<sub>2</sub>, 94 % N<sub>2</sub>, and 5 % CO<sub>2</sub>. The procedure started with centrifuging the culture medium at 300

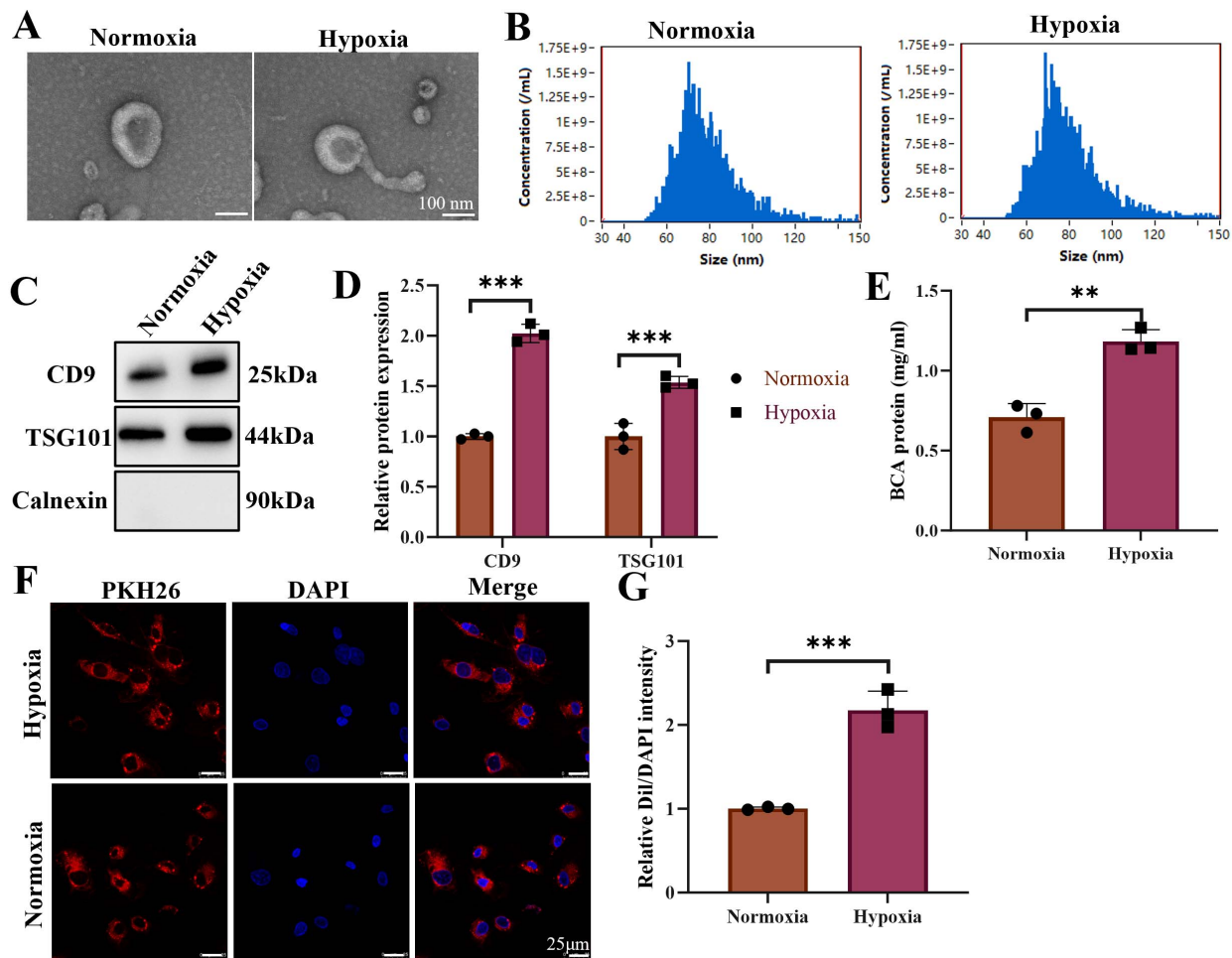


**Fig. 1. Hypoxia promoted exosome release from HucMSC.** (A) Morphology of Exos and hypoxia under TEM. Scale bar: 100 nm. (B) NTA analysis of Exos and hypoxia. (C,D) Western blot analysis of TSG101 and CD9 exosomal proteins. (E) The concentration of exosomal protein was determined by BCA method. (F) Immunofluorescence staining of PKH26 in normoxic and hypoxic HucMSC. Scale bar: 25  $\mu$ m. (G) Fluorescence intensity of PKH26. HucMSCs, human umbilical cord MSCs; TEM, transmission electron microscopy; NTA, nanoparticle tracking analysis. N = 3. \*\* $p$  < 0.01, \*\*\* $p$  < 0.001. DAPI, 4',6-diamidino-2-phenylindole; BCA, bicinchoninic acid assay.

g for 10 min followed by centrifugation at 2000 g for 10 min at 4 °C to further clear the medium of cells and debris. Afterwards, the medium was passed through a 0.22  $\mu$ m sterile filter (Steritop™, Millipore, Burlington, MA, USA) to remove any remaining cells and debris. The clarified supernatant was first condensed to around 200  $\mu$ L using an Amicon Ultra-15 centrifugal filter device (Merck Millipore, Billerica, MA, USA) by centrifuging at 4000 g. After this concentration step, the sample was washed twice with phosphate buffer saline (PBS) and once again reduced to a 200  $\mu$ L volume. To isolate exosomes, this treated supernatant was then layered over a 30 % sucrose/deuterium oxide (D<sub>2</sub>O) cushion in a sterile Ultra-Clear™ tube (344058, Beckman Coulter, Brea, CA, USA) and ultracentrifuged at 100,000 g for 60 min at 4 °C in an Optima L-100 XP Ultracentrifuge (Beckman Coulter, Brea, CA, USA). The exosome-dense layer (HucMSC-Exos) was carefully col-

lected using an 18-G needle, mixed with PBS, and condensed to 200  $\mu$ L through centrifugation at 4000 g and 4 °C. Subsequently, these exosomes were preserved at –80 °C for later use or immediately utilized in further experiments. Vesicle size for Exos and hypoxia was measured with a Nanosight LM10 System (Nanosight Ltd., Navato, CA, USA). Exosome shape from normoxic and hypoxic sources was analyzed using a transmission electron microscopy (TEM; Tecnai 12; Philips, Best, The Netherlands). The presence of markers like TSG101 and CD9 on the exosomes was checked by Western blotting. Protein levels in HucMSC-Exo were assessed using a bicinchoninic acid assay (BCA) protein assay kit (A55860, Thermo Fisher Scientific, Waltham, MA, USA), with absorbance noted at 562 nm using a microplate reader (ELx800; Bio-Tek Instruments, Inc., Winooski, VT, USA).

### Preparation of Naringin-Exosomes

Ng was provided by the China Institute for Drug and Biological Products Control (110722-200829, Beijing, China), and  $4 \times 10^6$  cells/mL density was suspended in PBS. About 50  $\mu\text{g}$  of Ng was added and extruded in a mini-extruder (610000, Avanti Polar Lipids Inc., Birmingham, AL, USA). Subsequently, the debris was removed by centrifugation, passed through a 0.2  $\mu\text{m}$  filter, and ultracentrifuged at  $1 \times 10^5$  g at 4 °C for 1 h.

### Ultraviolet-Visible (UV-Vis) Spectrophotometer Analysis Ng

UV-vis spectrophotometer was used to quantify Ng [29]. First, Ng with a concentration of 0–10  $\mu\text{g}/\text{mL}$  was prepared and the standard curve was generated. The presence of Ng in Ng-exosomes was verified by UV-vis spectrophotometry. Ng-exosomes were mixed with radioimmunoprecipitation assay (RIPA; P0013B, Beyotime Biotechnology, Shanghai, China) buffers and analyzed by UV absorbance at 230 nm wavelength. The protein in the sample was quantified with a BCA kit (P0009, Beyotime Biotechnology, Shanghai, China).

### Modeling Femur Breaks and Radiographic Evaluation

Femoral fracture model in mice was developed according to methods previously described in references [30]. Thirty-two C57BL 6/J male mice ( $20 \pm 5$  g), aged between 8–10 weeks, were anesthetized before making a small incision of around 10 mm to facilitate the insertion of a Kirschner wire into the femoral canal via the knee. Subsequently, a precise fracture was created at the mid-shaft of the femur using bone forceps. Pentobarbital sodium (1 %) anesthesia was administered to mice at a dose of 40 mg/kg. The mice were then divided into four groups (normoxic, hypoxic, normoxic with Ng concentration, and hypoxic with Ng concentration), with each group comprising eight mice. Ng-exosomes (200  $\mu\text{g}$  of total protein of exosomes precipitated in 200  $\mu\text{L}$  of PBS) were injected into the fracture site immediately after molding, followed by suturing of the incision. The progress of fracture healing was assessed seven days later with a Faxitron MX-20 X-ray system (Lincolnshire, IL, USA). For in-depth examination, the femurs were first fixed in 4 % paraformaldehyde for a 24 h, decalcified using 10 % ethylene diamine tetraacetic acid (EDTA) over 21 to 28 days, and finally prepared for evaluation by embedding them in paraffin. All mice were sacrificed by cervical dislocation.

### Microcomputed Tomography Imaging (Micro-CT)

The Kirschner wire was removed, and the femurs were preserved in 4 % paraformaldehyde for a day. Subsequently, they were imaged with a micro-CT scanner (SkyScan 1172, Bruker, Belgium, Germany) at a resolution of 18  $\mu\text{m}$ , with the machine set to 50 kV and 200  $\mu\text{A}$ . We generated three-dimensional reconstructions and eval-

uated the bone's morphometric features especially the mineralized callus volume/tissue volume (CV/TV) ratio using CT-Analyser software (3.0, CTAn, Bruker, Belgium, Germany).

### Immunofluorescence Staining

Tissue sections were treated with antibodies against CD31 (ab76533, Abcam, Cambridge, MA, USA) and Ki-67 (ab16667, Abcam, Cambridge, MA, USA) to perform double immunofluorescence staining. This process involved an overnight incubation at 4 °C followed by exposure to secondary antibodies conjugated with Alexa Fluor 488 and Alexa Fluor 594 (1:200, Jackson ImmunoResearch, West Grove, PA, USA) for 1 h at ambient temperature. After three PBS washes, the cell nuclei were highlighted using 4',6-diamidino-2-phenylindole (62248, Thermo Fisher Scientific, Waltham, MA, USA). Fluorescent microscopy (AxioVert A1 and Imager A2, Zeiss, Oberkochen, Baden-Württemberg, Germany) was then used to capture the stained images.

A cell-membrane staining kit (D0030, Solarbio, Beijing, China) was used for PKH26 staining analysis. About  $2 \times 10^7$  cells were centrifuged in a conical centrifuge tube at 400 g for 5 min. The supernatant was discarded, and 1 mL of diluent C paper cup  $2 \times$  cell suspension was added. Then, 4  $\mu\text{L}$  of PKH26 ethanol solution was added into 1 mL of diluent C, thoroughly mixed, and incubated at 25 °C for 5 min. After adding 1 % bovine serum albumin (BSA) to stop the staining reaction, centrifuging for 10 min at 25 °C and 400 g, and cleaning twice with complete medium, the samples were observed under microscope (CX41-32RFL, Olympus Corporation, Tokyo, Japan).

### siRNA Transfection

siRNA targeting the gene was sourced from Santa Cruz Biotechnology, comprising a mix of six siRNAs, each 20 to 25 nucleotides in length, aimed at reducing gene expression. During transfection, 60 pmol of siRNA prepared in siRNA transfection medium (sc-36868, Santa Cruz Biotechnology, Santa Cruz, CA, USA), was mixed with 6  $\mu\text{L}$  of siRNA transfection reagent (sc-108061, Santa Cruz Biotechnology, Santa Cruz, CA, USA) that had been equally mixed with the transfection medium beforehand. This combination was left to settle at room temperature for 30 min before further diluting with the transfection medium and applying to HucMSCs on a six-well plate. Following an 8 h incubation, the cells were maintained in full growth medium for an additional 48 h and then analyzed through immunofluorescence. Integrin  $\beta 1$  siRNA: sense: 5'-UAGAUUAUCUCGCGUCAUACdTdT-3' and anti-sense: 5'-GUAUGACGCGAGAUUAUCUAdTdT-3'; TRKB siRNA: sense: 5'-GAAUUGACGAUGGUGCAAAt; antisense: 5'-UUUGCACCAUCGUCAAUUCca.

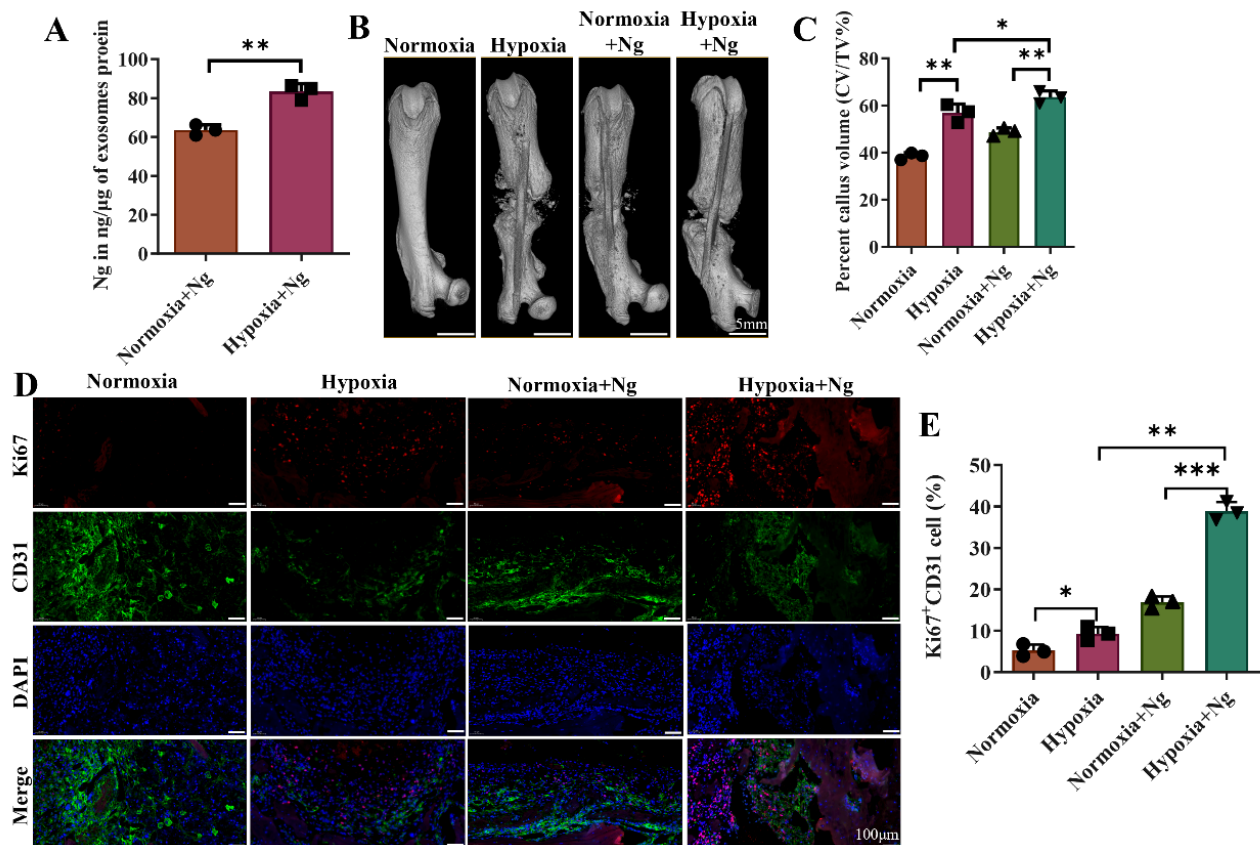


**Fig. 2. Bone-fracture healing was promoted in mice after the transplantation of hypoxia + Ng.** (A) Ng load efficiency. (B) Representative three-dimensional micro-CT images of a mouse femur fracture model on the 7th day after fracture. Scale bar: 5 mm. (C) Statistical analysis of mineralized callus volume/tissue volume (CV/TV) % from micro-CT scanning (N = 8). (D) Immunofluorescence staining of Ki-67 (red) and CD31 (green) in callus on day 7 after fracture. Scale bar: 100  $\mu$ m. (E) Quantification of positive Ki67<sup>+</sup>/CD31<sup>+</sup> cells. Ng, Naringin; micro-CT, microcomputed tomography imaging. N = 3. \* $p$  < 0.05, \*\* $p$  < 0.01, \*\*\* $p$  < 0.001.

#### Cell Counting Kit-8 (CCK8) Assay

The proliferation rate of cells was determined using a CCK8 assay kit (CK04) from Dojindo, Kumamoto, Japan. Initially, HucMSCs were distributed at 2000 cells per well in 100  $\mu$ L of culture medium across a 96-well plate. These cells were then exposed to different conditions: normoxic, hypoxic, normoxic with Ng mixture, and hypoxic with Ng mixture.

#### 5-Ethynyl-2'-Deoxyuridine (EdU) Assay

Cell proliferation was evaluated using an EdU assay kit (C10310) from RiboBio, Guangzhou, China, adhering to the instructions included. In a typical procedure, cells were seeded onto 24-well plates at a density of 20,000 cells per well and cultured for 24 h. Afterwards, EdU (50 mM) was added to the cells. Following EdU incorporation, cells were stained using Apollo for EdU detection and additional DNA staining. Cell proliferation was then observed and quantified through fluorescence microscopy (CX41-32RFL, Olympus Corporation, Tokyo, Japan). Furthermore, cell-growth rates were assessed using an iClick<sup>TM</sup> EdU Andy Fluor 647 flow cytometry assay

kit (A008, ABP Biosciences, Rockville, MD, USA) per the manufacturer's guidelines. The proportion of EdU-positive cells was calculated using flow cytometry (FACS-Calibur; BD Biosciences, Franklinho, NJ, USA).

#### Tube-Formation Assay

The angiogenic ability of Exos and hypoxia was evaluated by culturing HucMSCs at a concentration of 20,000 cells per well on 96-well plates precoated with matrigel. The process began with the application of a 50  $\mu$ L Matrigel layer on each well, using tips that were cooled to 4  $^{\circ}$ C. After the Matrigel had hardened, 100  $\mu$ L of a HucMSC blend treated with normoxic, hypoxic, normoxic with Ng concentration, or hypoxic with Ng was added on top and then incubated for an additional 30 min at 37  $^{\circ}$ C. The formation of capillary-like structures was observed under a light microscope (LV150, Nikon, Tokyo, Japan). Special attention was paid to the polygonal formations that appeared 6 h after planting. The total length of these structures was measured by analyzing five random fields per well using ImageJ software (V1.8, National Institutes of Health, Bethesda, MD, USA).

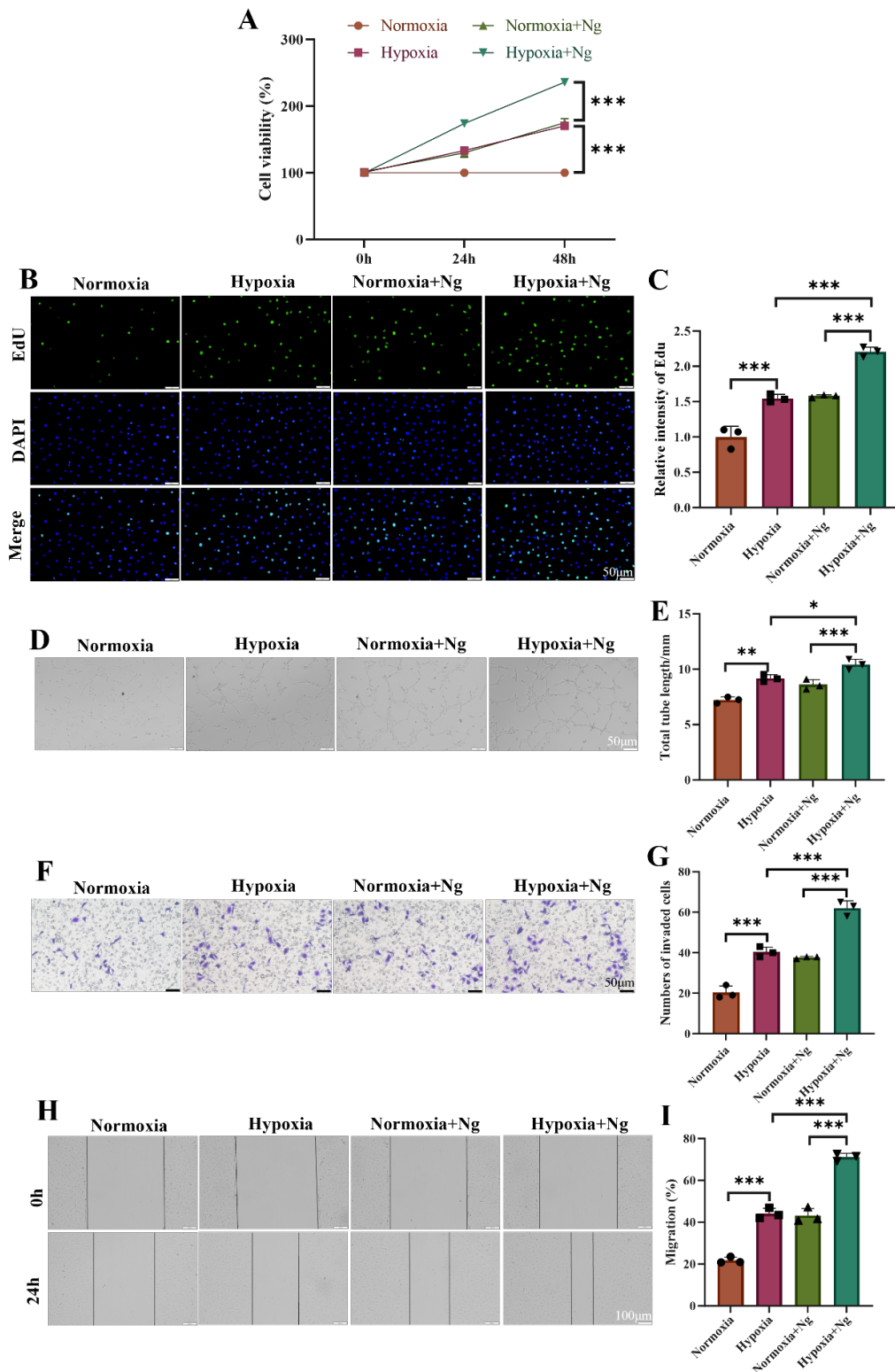


**Fig. 3. Hypoxia + Ng promoted proliferation, migration, and tube formation in recipient HucMSCs *in vitro*.** (A) HucMSCs proliferation after normoxia, hypoxia, normoxia + Ng, and hypoxia + Ng as measured by CCK8 assay. (B,C) HucMSCs proliferation measured by EdU staining. Scale bar: 50  $\mu$ m. (D,E) Representative images and quantitative analysis showed tube formation in HucMSCs treated with normoxia, hypoxia, normoxia + Ng, and hypoxia + Ng. Scale bar: 50  $\mu$ m. (F,G) Representative images and quantitative analysis showed invaded HucMSCs. Scale bar: 50  $\mu$ m. (H,I) Representative images and quantitative analysis showed the migration ability of HucMSCs. Scale bar: 100  $\mu$ m. EdU, 5-ethynyl-2'-deoxyuridine; CCK8, cell counting kit-8. N = 3. \* $p$  < 0.05, \*\* $p$  < 0.01, \*\*\* $p$  < 0.001.

### Migration Assay

The influence of Exos and hypoxia on the migration of HucMSCs was evaluated using a Transwell assay. In this setup, 20,000 HucMSCs were placed on the top chamber of a 24-well Transwell plate (7424, Corning Incorporated, Corning, NY, USA) equipped with 8  $\mu\text{m}$  pores. The bottom chamber was supplied with 600  $\mu\text{L}$  of medium treated in various ways to promote cell migration. Following a 24 h incubation period, cells that had not traversed the membrane were removed from the upper surface by using a cotton swab. Migrated cells on the membrane's lower side were then stained with 0.5 % crystal violet for 1 min. The tally of cells that had migrated was accomplished by visual inspection and counting of the stained cells with a light microscope.

Additionally, a scratch assay was utilized to further assess cell migration. HucMSCs were initially cultivated on six-well plates until they reached a confluent monolayer ( $2 \times 10^5$  cells per well). A sterile 200  $\mu\text{L}$  pipette tip was used to make a scratch through the layer of cells. Subsequently, the wells were rinsed three times with PBS to remove any cells that had been dislodged, and treatments with either PBS, 100  $\mu\text{g}/\text{mL}$  of Exos, or hypoxia were administered. The healing of the scratch, serving as an indicator of cell migration, was monitored at 0 and 12 h post-scratch.

### Western Blot Analysis

Proteins were isolated using RIPA lysis (R0010, Solarbio, Beijing, China), with their concentrations measured by a BCA protein assay kit (PC0020, Solarbio, Beijing, China). Following the determination of protein levels, the samples were subjected to sodium dodecyl sulfate polyacrylamide gel electrophoresis (SDS-PAGE) and then transferred onto polyvinylidene fluoride (PVDF) membranes (IPVH00010, Millipore Corporation, Billerica, MA, USA). After incubating the membranes with primary antibodies overnight at 4 °C and subsequently blocked with 5 % BSA, secondary antibodies were then applied for 2 h at ambient temperature. Bands were detected using an enhanced chemiluminescence (ECL) reagent (BL520b, Biosharp Life Science, Hefei, China), and the intensity of these bands was evaluated semi-quantitatively using ImageJ software (V1.8, National Institutes of Health, Bethesda, MD, USA). The primary antibodies used included anti-CD9 (sc-20048), anti-calnexin (sc-80645) and anti-TSG101 (sc-101254) at a dilution of 1:500 (Santa Cruz Biotechnology, Santa Cruz, CA, USA); anti-BDNF (ab108319), anti-TrkB (ab187041), and anti-glyceraldehyde-3-phosphate dehydrogenase (GAPDH) (ab8245) at a dilution of 1:1000 (Abcam, Cambridge, MA, USA); and anti-ERK1/2 (4695), along with anti-phospho-ERK1/2 (4370) at a dilution of 1:1000 (Cell Signaling Technology, Boston, MA, USA).

### Statistical Analysis

Data are shown as mean  $\pm$  standard deviation from at least three separate experiments. Statistical analysis was conducted using GraphPad Prism (version 7.0, Graph-Pad Software, San Diego, CA, USA) and SPSS (version 19.0, IBM Corporation, Armonk, NY, USA). For comparing two groups, the Student's *t*-test was applied, whereas one-way or two-way analysis of variance (ANOVA) with Bonferroni correction was used for multiple-group comparisons. Significance was determined by a *p* value less than 0.05. Significance levels were denoted as \* for *p* < 0.05, \*\* for *p* < 0.01, and \*\*\* for *p* < 0.001.

## Results

### Identification of Exosomes Derived from Hypoxic in HucMSCs

The exosomes were thoroughly characterized through techniques such as electron microscopy, nanoparticle tracking analysis (NTA), and Western blotting. TEM revealed that the exosomes were generally spherical, with diameters ranging from 50 nm to 200 nm (Fig. 1A). NTA confirmed this size range, showing average sizes of 75.25 nm under normoxic conditions and 72.75 nm under hypoxic ones, without significant differences in morphology including size, shape, or electron density among the two groups. However, the addition of Ng to the hypoxic environment significantly increased the number of nanoparticles compared with the hypoxic group without Ng (Fig. 1B). Fig. 1C,D showed exosome-specific markers such as TSG101 and CD9, whereas calnexin was undetected. Moreover, the protein content in exosomes from hypoxic HucMSC was notably greater (*p* < 0.01, Fig. 1E). Fig. 1F,G shows that exposure to hypoxic conditions also resulted in a significantly higher exosome release than the normoxic baseline (*p* < 0.001).

### Acceleration of Bone-Fracture Healing in Mice via Transplantation with Ng-Loaded Hypoxic Exosomes

Fig. 2A shows that the loading efficiency of NG-exosomes in normoxia was 63.57 ng/mg and that in hypoxia was 83.40 ng/mg. Micro-CT was used for scanning, and reconstruction allowed for a qualitative evaluation of callus volumes on the seventh day post-surgery (Fig. 2B,C). The hypoxia + Ng group resulted in a notable rise in the CV/TV ratio (*p* < 0.01). In Fig. 2D,E, endothelial cell proliferation increased in the hypoxia + Ng group (*p* < 0.001). Overall, these findings emphasized that the application of hypoxia + Ng promoted angiogenesis, significantly advancing bone healing *in vivo*.

### Hypoxia + Ng Promoted Proliferation, Migration, and Tube Formation in HucMSCs

To evaluate whether hypoxia + Ng provided similar therapeutic benefits *in vitro* as observed *in vivo*, we treated HucMSCs with normoxia, hypoxia, normoxia + Ng, and

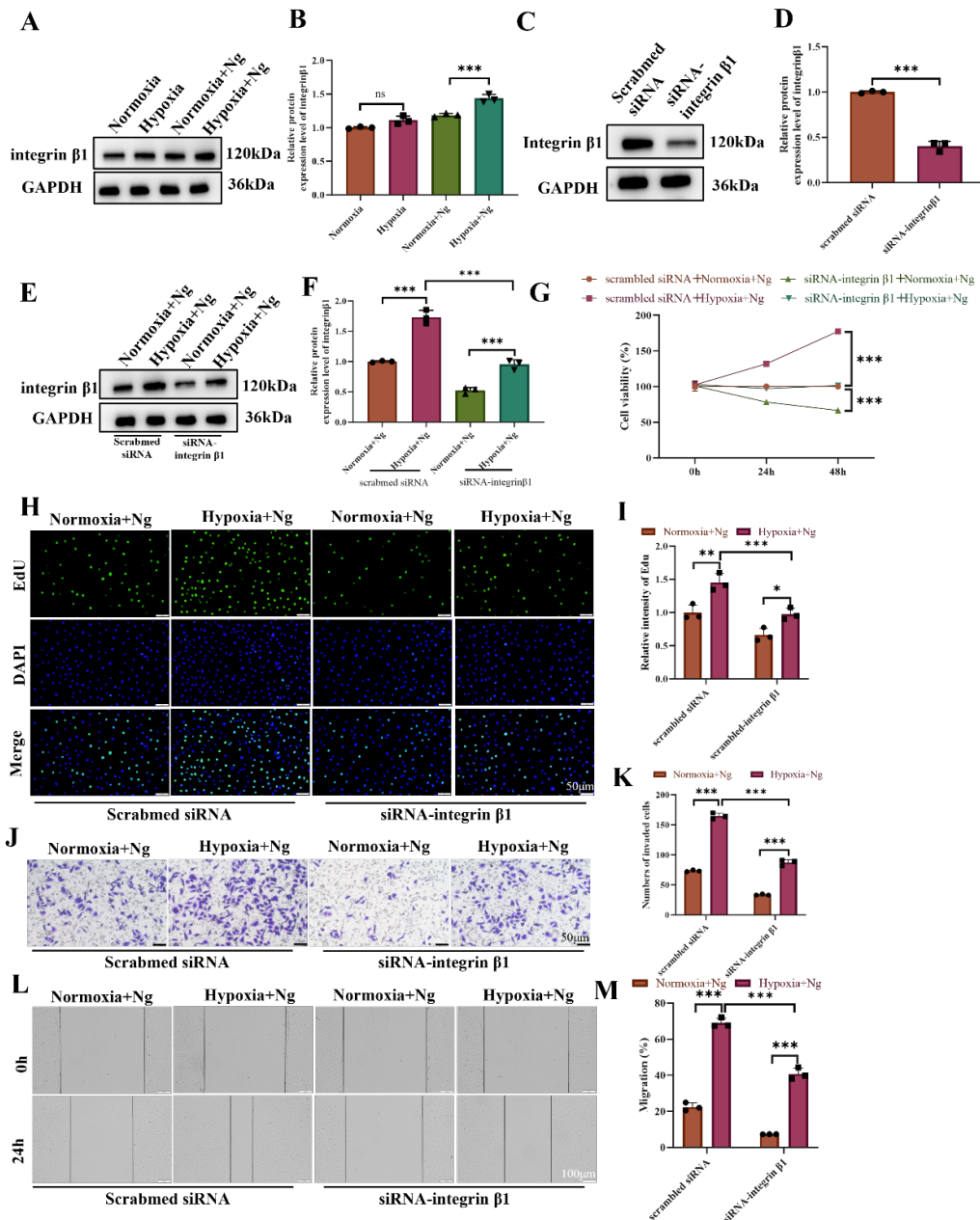


**Fig. 4. Inhibited integrin  $\beta 1$  significantly reduced proliferation, migration, and tube formation in HucMSCs.** (A,B) Protein expression of integrin  $\beta 1$  in HucMSCs after normoxia, hypoxia, normoxia + Ng, and hypoxia + Ng. (C,D) Protein expression of integrin  $\beta 1$  in knockdown experiment. (E,F) Protein expression of integrin  $\beta 1$  in HucMSCs transfected with scrambled siRNA or siRNA-integrin  $\beta 1$ . (G) Cell proliferation. (H,I) Cell proliferation of HucMSCs measured by EdU staining. Scale bar: 50  $\mu$ m. (J) Representative images showing Transwell invasion in HucMSCs treated with normoxia, hypoxia, normoxia + Ng, and hypoxia + Ng. Scale bar: 50  $\mu$ m. (K) Quantitative analysis of Transwell invasion assay. (L) Representative images showing migrated HucMSCs. Scale bar: 100  $\mu$ m. (M) Quantitative analysis of migrated cells. GAPDH, glyceraldehyde-3-phosphate dehydrogenase. N = 3, ns, no statistical difference; \* $p$  < 0.05, \*\* $p$  < 0.01, \*\*\* $p$  < 0.001.

hypoxia + Ng. Fig. 3A illustrates a significant enhancement in HucMSC proliferation following incubation with hypoxia + Ng ( $p$  < 0.001). According to the results of EdU assay, as shown in Fig. 3B,C, the number of EdU-positive HucMSCs was significantly higher in the hypoxia + Ng group than in the normoxia + Ng ( $p$  < 0.001) and hypoxia

( $p$  < 0.001) groups. The formation of capillary tubes by HucMSCs was monitored, and tube lengths were measured, showing that hypoxia + Ng significantly enhanced tube formation 6 h post-treatment compared with the hypoxia group ( $p$  < 0.05) (Fig. 3D,E). Additionally, cells treated with hypoxia + Ng demonstrated superior tube-formation capa-

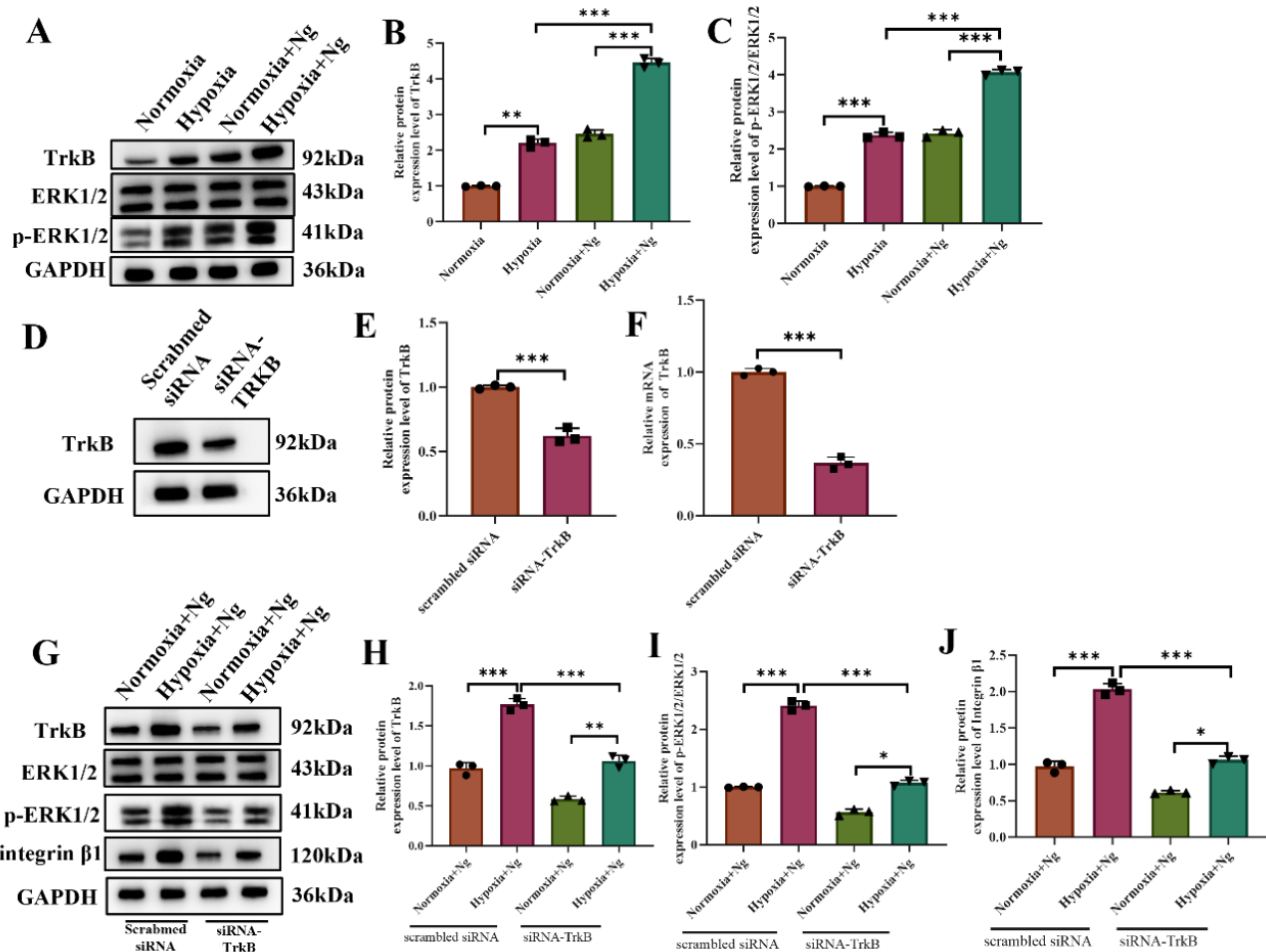


**Fig. 5. TrkB/ERK1/2 pathway played an important role in regulating integrin  $\beta 1$  and in promoting osteoblast migration and bone-fracture healing.** (A–C) Protein expression of TrkB, p-ERK1/2/ERK1/2 in HucMSCs after normoxia, hypoxia, normoxia + Ng, and hypoxia + Ng. (D–F) Protein expression of TrkB in knockdown experiment. (G–J) Protein expression of TrkB, p-ERK1/2/ERK1/2, integrin  $\beta 1$ . ERK, extracellular regulated protein kinases; TrkB, tropomyosin receptor kinase B. N = 3, \* $p < 0.05$ , \*\* $p < 0.01$ , \*\*\* $p < 0.001$ .

bilities relative to those treated with the normoxia + Ng ( $p < 0.001$ ). Transwell (Fig. 3F,G) and scratch assays (Fig. 3H,I) were used to evaluate how exosomes influenced the migration of HucMSCs. The findings confirmed that hypoxia + Ng facilitated HucMSC migration beyond that of the normoxia + Ng treatment ( $p < 0.001$ ). In summary, these *in vitro* experiments demonstrated that hypoxia + Ng markedly promoted HucMSC proliferation, migration, and tube-formation capabilities, surpassing the effects of normoxia + Ng and standard hypoxia treatment.

*Inhibited Integrin  $\beta 1$  Significantly Reduced Proliferation, Migration, and Tube Formation in HucMSCs*

Integrins are heterodimeric transmembrane receptors formed by the assembly of  $\alpha$  and  $\beta$  subunits. They play crucial roles in cell-to-cell and cell-to-matrix interactions. In particular, integrin  $\beta 1$  is a key component in osteoblasts. In our study, hypoxia + Ng further amplified the protein expression of integrin  $\beta 1$  more markedly than did hypoxia

( $p < 0.001$ ) (Fig. 4A,B). Further investigations were conducted by knocking down integrin  $\beta 1$  to validate its function. Results from Western blot and mRNA analyses indicated a significant reduction in the expression of integrin  $\beta 1$  in the exosomes ( $p < 0.001$ ) (Fig. 4C–F). Additionally, CCK8 ( $p < 0.001$ ) and EdU assays ( $p < 0.001$ ) revealed that the knockdown of integrin  $\beta 1$  significantly reduced cell proliferation in HucMSCs (Fig. 4G–I). This finding was further corroborated by Transwell and scratch assays, demonstrating that inhibited integrin  $\beta 1$  notably decreased proliferation, migration, and invasion in HucMSCs ( $p < 0.001$ ) (Fig. 4J–M). Overall, results indicated that hypoxia-derived MSC exosomes delivering Ng enhanced osteoblast migration and fracture healing by upregulating Integrin  $\beta 1$ .

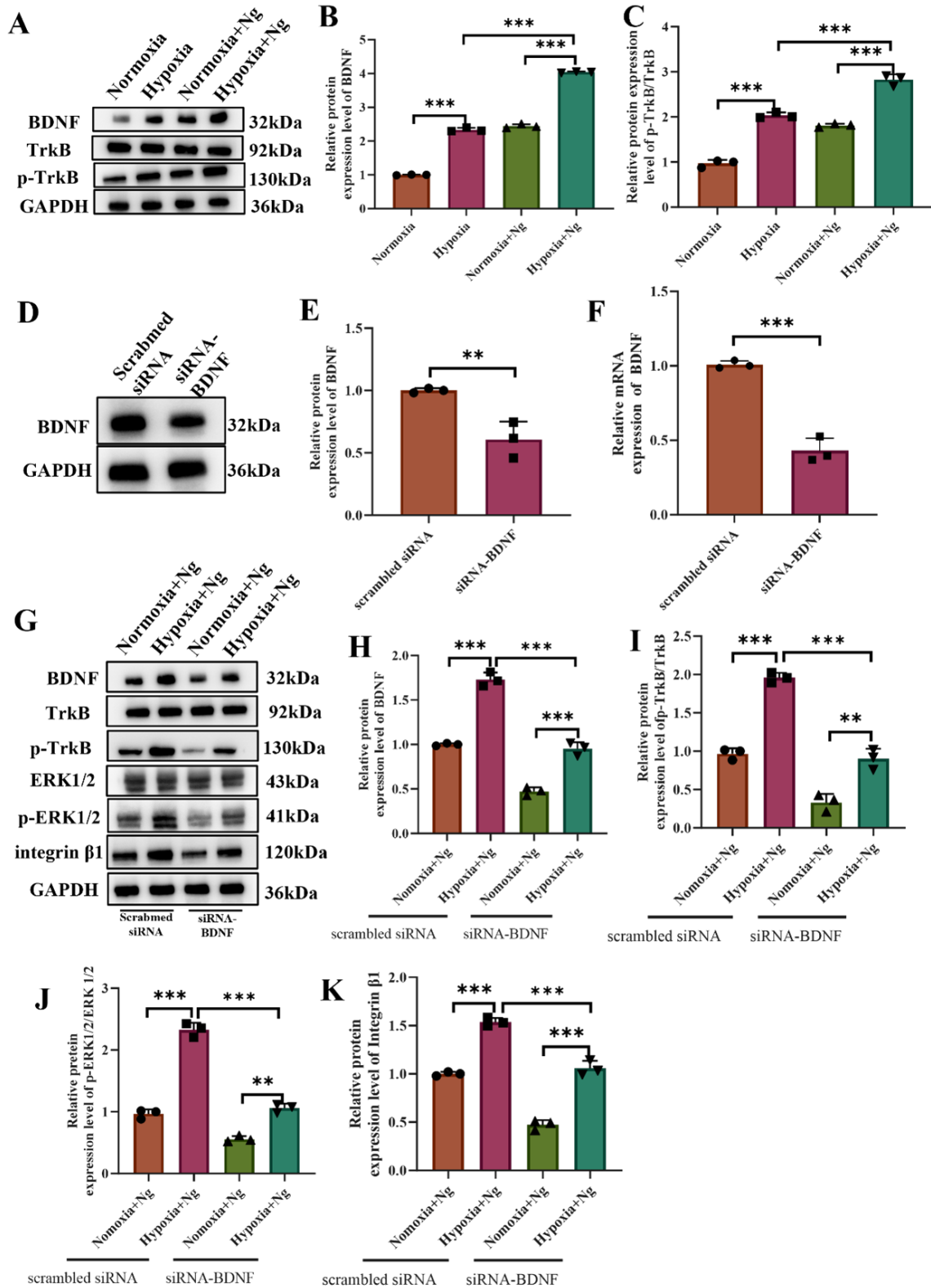


**Fig. 6. BDNF promoted osteoblast migration and fracture healing by upregulating integrin  $\beta 1$  via the TrkB-mediated ERK1/2 pathway.** (A–C) Protein expression of BDNF, p-TrkB/TrkB, p-ERK1/2/ERK1/2 in HUCMSCs after normoxia, hypoxia, normoxia + Ng, and hypoxia + Ng. (D–F) Protein expression of BDNF in knockdown experiment. (G–K) Protein expression of BDNF, TrkB, p-ERK1/2/ERK1/2, integrin  $\beta 1$ . BDNF, brain-derived neurotrophic factor. N = 3, \*\* $p < 0.01$ , \*\*\* $p < 0.001$ .

### *TrkB/ERK1/2 Pathway Played an Important Role in Regulating Integrin $\beta$ 1 and in Promoting Osteoblast Migration and Bone-Fracture Healing*

The TrkB/ERK1/2 pathway reportedly plays a crucial role in regulating integrin  $\beta$ 1. To further explore the molecular mechanisms through which hypoxia + Ng regulated osteoblast migration and bone-fracture healing, we observed the protein levels of TrkB and the p-ERK1/2/ERK1/2. Protein levels of TrkB ( $p < 0.01$ ) and p-ERK1/2/ERK1/2 were found to increase ( $p < 0.001$ ) in the hypoxia group compared with the normoxia group (Fig. 5A–C). Moreover, hypoxia + Ng further amplified the protein expression of TrkB and p-ERK1/2/ERK1/2 more markedly than did hypoxia ( $p < 0.001$ ) (Fig. 5A–C). To further investigate the function and impact of the TrkB/ERK1/2 pathway in regulating integrin  $\beta$ 1, our findings from mRNA and Western blot analyses demonstrated the successful knockdown of TrkB expression by using siRNA ( $p < 0.001$ ) (Fig. 5D–F). Subsequently, we observed a significant reduction in the protein expression of phosphorylated and total ERK1/2 (p-ERK1/2/ERK1/2) following the siRNA-mediated knockdown of TrkB ( $p < 0.001$ ) (Fig. 5G–I). This reduction was accompanied by a notable decrease in the expression of integrin  $\beta$ 1 ( $p < 0.001$ ) (Fig. 5J). Therefore, Ng, via exosomes and the TrkB/ERK1/2 pathway, regulated integrin  $\beta$ 1 to promote osteoblast migration and bone-fracture healing.

### *BDNF Promoted Osteoblast Migration and Fracture Healing by Upregulating Integrin $\beta$ 1 via the TrkB-Mediated ERK1/2 Pathway*

BDNF, a pivotal player in the neurotrophin family, significantly influences the survival, development, and functionality of neurons. Acting through its specific receptor, TrkB, BDNF plays a crucial role. TrkB is distinguished by its unique transmembrane portion and an intracellular domain, noted for its Trk activity. This interaction between BDNF and TrkB is fundamental in neurobiology, affecting various aspects of neural health and disease mechanisms. BDNF facilitates osteoblast migration and bone-fracture repair through its interaction with the TrkB receptor and the extracellular regulated protein kinases 1/2 (ERK1/2) signaling pathway. In the context of our research on the modulatory effects of hypoxia + Ng on osteoblast migration and bone-fracture consolidation, BDNF emerged as a critical mediator (Fig. 6A–C). Experimental outcomes demonstrated an upregulation in BDNF protein expression within the hypoxia group relative to the normoxia cohort. Notably, hypoxia + Ng induced a more pronounced enhancement of BDNF protein expression than hypoxia alone ( $p < 0.001$ ). Additionally, our application of siRNA technology to suppress BDNF expression ( $p < 0.01$ ) resulted in markedly decreased BDNF levels in HucMSCs ( $p < 0.001$ ) (Fig. 6D–F), accompanied by a significant reduction in the protein levels of TrkB and the phosphorylated-to-total

ERK ratio ( $p < 0.01$ ) (Fig. 6G–K). This was concomitant with a significant downregulation of integrin  $\beta$ 1 expression post-BDNF knockdown ( $p < 0.001$ ). These findings indicated that under hypoxic conditions, MSC-derived exosomes, serving as vectors for hypoxia + Ng, specifically targeted the BDNF/TrkB-ERK1/2 signaling axis. The outcome was upregulated integrin  $\beta$ 1, thereby enhancing osteoblast migration and facilitating bone-fracture healing.

In summary, our study provided compelling evidence that hypoxia + Ng augmented osteoblast migration and bone-fracture repair by upregulating integrin  $\beta$ 1 via the BDNF/TrkB/ERK1/2 signaling pathway, underscoring its potential therapeutic application in bone-repair strategies.

## Discussion

Stem-cell transplantation holds promise for treating stubborn diseases owing to their self-renewal and differentiation capabilities [31]. However, challenges such as low targeting efficiency to tissues and reduced function in age-related disorders remain. Ng, a bioactive compound from traditional Chinese medicine, influences osteoblast and osteoclast functions. It shows potential in enhancing BDNF and VEGF expression in injury models [32,33]. Nevertheless, the specific effects and mechanisms of Ng in MSC-derived exosomes for bone repair require further exploration, suggesting a new avenue for cellular therapy.

Existing research suggests that the beneficial effects of transplanted MSCs largely originate from their ability to secrete biologically active molecules, a process known as paracrine signaling [34]. Compared with direct MSC transplantation, exosomes derived from these cells have demonstrated therapeutic potential across a range of conditions including osteonecrosis, organ failures, traumatic injuries, myocardial infarction, ischemic diseases, and chronic wounds [35]. The discrepancy between *in vitro* oxygen levels (21 % O<sub>2</sub> under standard culture conditions) and the *in vivo* physiological environment, which does not accurately replicate tissue microenvironments, is notable [36,37]. Furthermore, MSCs subjected to hypoxic conditions have shown enhanced biological functions and therapeutic outcomes, highlighting the significance of the hypoxic microenvironment prevalent in various inflamed or diseased tissues [38,39]. This necessitates a detailed examination of cellular behaviors in normoxic versus hypoxic environments. Consequently, in our investigation, we devised a robust murine model for bone fracture and proposed the following: (1) exosomes harvested from MSCs cultivated in hypoxic conditions, and incorporating Ng, deliver superior therapeutic advantages compared with those derived from MSCs cultured at normoxic (standard oxygen) levels; and (2) the biological mechanisms through which exosomes, originating from MSCs under hypoxic conditions and laden with Ng, facilitated the healing of bone fractures were delineated.

The human umbilical cord is acknowledged as one of the many sources of MSCs due to its affordable, abundant, and highly versatile potential; this is further corroborated by data showing the therapeutic advantages of exosomes derived from HucMSCs under a variety of medical situations [40]. Notably, a recent study has demonstrated the protective function of HucMSC-derived exosomes against cisplatin-induced renal oxidative damage, their ability to mitigate hepatic ischemia-reperfusion injury in rats, their capacity to attenuate scar formation during wound healing, and their ability to promote angiogenesis in rat models of myocardial infarction [41]. He *et al.* [42] further highlighted the angiogenic potential of HucMSC-derived exosomes in bone-fracture healing contexts, yet the precise mechanistic underpinnings remain to be fully elucidated. After bone fracture, the hypoxic conditions faced by MSCs are exacerbated. This scenario is difficult to mimic accurately *in vitro*, so our investigation embarked on a comprehensive series of *in vivo* and *in vitro* assays to substantiate our hypothesis. Analytical assessments through TEM and NTA revealed no notable variances in the morphological attributes, namely, size, shape, or electron density, among exosomes derived under normoxia, hypoxia, normoxia + Ng, and hypoxia + Ng. However, subsequent investigations revealed that hypoxic environments notably facilitated the augmented release of exosomes from HucMSCs. Our preliminary findings, encompassing *in vitro* and *in vivo* paradigms, suggested that the transplantation of HucMSC-derived exosomes with Ng notably promoted cellular proliferation, angiogenesis, and migration. These therapeutic outcomes were significantly enhanced in the hypoxia cohort.

Integrins, identified as  $\alpha/\beta$  heterodimeric membrane receptors, are essential in modulating cell migration, differentiation, and proliferation through their interactions with several extracellular matrix ligands, including fibronectin, vimentin, and collagen. Their role in facilitating growth factor signaling pathways is also well documented [43]. In our research, we noted a significant increase in integrin  $\beta 1$  expression when cells were subjected to hypoxia and treated with Ng. Subsequent experiments using siRNA to reduce integrin  $\beta 1$  levels led to a noticeable decrease in the proliferation, migration, and tube-formation capabilities of HucMSCs. These findings highlighted the influence of hypoxia + Ng in promoting osteoblast migration and bone-fracture healing through integrin  $\beta 1$  upregulation. BDNF also raised the integrin  $\beta 1$  levels in HucMSCs, with integrin  $\beta 1$  mitigating the BDNF-induced migration of these cells. Inhibiting the TrkB/ERK pathway decreased integrin  $\beta 1$  expression. Similarly, Zhang *et al.* [28] reported that BDNF boosts osteoblast migration and speeds up fracture healing by elevating integrin  $\beta 1$  through the activation of TrkB-mediated ERK1/2 and AKT signaling. BDNF reportedly promotes fracture healing through TrkB-mediated ERK signaling [28] and promotes osteoblast se-

cretion [44]. When BDNF binds to TrkB, it activates the receptor's tyrosine kinase activity, which triggers its intracellular signaling cascade such as the ERK1/2 and AKT pathways, two important kinases that regulate cell movement [45,46]. Through the TrkB/ERK1/2 pathway, BDNF promotes cell proliferation and migration [47,48]. However, studies on the relationship between integrins and BDNF are few. In the process of chondrosarcoma migration promoted by BDNF, integrin  $\beta 5$  was upregulated through the TrkB/AKT signaling cascade, whereas in the process of microvascular endothelial cell migration mediated by BDNF integrin  $\beta 3$  was upregulated through the TrkB/ERK1/2 pathway [48,49]. Therefore, our findings strongly suggested that hypoxia + Ng enhanced osteoblast migration and bone healing by modulating integrin  $\beta 1$  via the BDNF/TrkB/ERK signaling axis, highlighting its therapeutic potential in bone-healing interventions. Additionally, oxidative stress and neuroinflammation can be alleviated through the BDNF/TrkB/ERK signaling pathway [50]. This can provide an idea for more extensive research in the future.

Our study had many shortcomings. First, the sample size was small, and it should be expanded in future studies. Additionally, clinical samples were not used, so clinical samples should be involved in subsequent studies to enrich the types of samples and further prove the drawn conclusions. Finally, future studies should also explore the link between other pathways and existing findings, as well as the implications of this study for other diseases.

## Conclusions

Our study offered strong evidence that MSC-derived exosomes, particularly those from HucMSCs under hypoxic conditions supplemented with Ng, hold considerable promise for enhancing bone-fracture healing. This effect is mediated by the upregulation of integrin  $\beta 1$  via the BDNF/TrkB/ERK signaling pathway, highlighting the therapeutic potential of hypoxia + Ng in bone-repair strategies and suggesting a novel avenue for cellular therapy in treating stubborn diseases.

## List of Abbreviations

MSCs, mesenchymal stem cells; TEM, transmission electron microscopy; NTA, nanoparticle tracking analysis; Ng, Naringin; micro-CT, microcomputed tomography imaging; CCK8, cell counting kit-8; EdU, 5-ethynyl-2'-deoxyuridine; PVDF, polyvinylidene fluoride; ECL, enhanced chemiluminescence; TrkB, tropomyosin receptor kinase B; BDNF, brain-derived neurotrophic factor; ERK, extracellular regulated protein kinases; GAPDH, glyceraldehyde-3-phosphate dehydrogenase; HucMSCs, human umbilical cord MSCs; FBS, fetal bovine serum; RIPA, radioimmunoprecipitation assay; CV/TV, callus volume/tissue volume; BSA, bovine serum albumin; ns, no statistical difference; UV-vis, Ultraviolet-visible;

DMEM, dulbecco's modified eagle medium; PBS, phosphate buffer saline; BCA, bicinchoninic acid assay; DAPI, 4',6-diamidino-2-phenylindole; VEGF, vascular endothelial growth factor.

### Availability of Data and Materials

The datasets used and/or analyzed during the current study are available from the corresponding author on reasonable request.

### Author Contributions

RFY and YYL contributed to the design of this work. HLT contributed to the interpretation of data. RFY and HLT analyzed the data. RFY and HLT drafted the work. YYL and HLT revised critically for important intellectual content. All authors read and approved the final manuscript. All authors agreed to be accountable for all aspects of this work, ensuring that questions related to the accuracy or integrity of any part of the work were appropriately investigated and resolved.

### Ethics Approval and Consent to Participate

Protocol was approved by the Institutional Animal Care and Use Committee of Shandong Academy of Pharmaceutical Sciences (IACUC-care-2024024) in accordance with Guide for the Care and Use of Laboratory Animals, 8th edition (National Research Council, 2010).

### Acknowledgments

Not applicable.

### Funding

Not applicable.

### Conflict of Interest

The authors declare no conflict of interest.

### References

- [1] Zhang F, Huan L, Xu T, Li G, Zheng B, Zhao H, *et al.* Inflammatory macrophages facilitate mechanical stress-induced osteogenesis. *Aging*. 2020; 12: 3617–3625. <https://doi.org/10.18632/aging.102833>.
- [2] Dai G, Xiao H, Liao J, Zhou N, Zhao C, Xu W, *et al.* Osteocyte TGF $\beta$ 1-Smad2/3 is positively associated with bone turnover parameters in subchondral bone of advanced osteoarthritis. *International Journal of Molecular Medicine*. 2020; 46: 167–178. <https://doi.org/10.3892/ijmm.2020.4576>.
- [3] Salhotra A, Shah HN, Levi B, Longaker MT. Mechanisms of bone development and repair. *Nature Reviews. Molecular Cell Biology*. 2020; 21: 696–711. <https://doi.org/10.1038/s41580-020-00279-w>.
- [4] Chen W, Wu P, Yu F, Luo G, Qing L, Tang J. HIF-1 $\alpha$  Regulates Bone Homeostasis and Angiogenesis, Participating in the Occurrence of Bone Metabolic Diseases. *Cells*. 2022; 11: 3552. <https://doi.org/10.3390/cells11223552>.
- [5] Dabrowska S, Del Fattore A, Karnas E, Frontczak-Baniewicz M, Kozłowska H, Muraca M, *et al.* Imaging of extracellular vesicles derived from human bone marrow mesenchymal stem cells using fluorescent and magnetic labels. *International Journal of Nanomedicine*. 2018; 13: 1653–1664. <https://doi.org/10.2147/IJN.S159404>.
- [6] Songsaad A, Gonmanee T, Ruangsawasdi N, Phruksaniyom C, Thonabulsombat C. Potential of resveratrol in enrichment of neural progenitor-like cell induction of human stem cells from apical papilla. *Stem Cell Research & Therapy*. 2020; 11: 542. <https://doi.org/10.1186/s13287-020-02069-9>.
- [7] Liu J, Zhu P, Song P, Xiong W, Chen H, Peng W, *et al.* Pretreatment of Adipose Derived Stem Cells with Curcumin Facilitates Myocardial Recovery via Antiapoptosis and Angiogenesis. *Stem Cells International*. 2015; 2015: 638153. <https://doi.org/10.1155/2015/638153>.
- [8] Zhao S, Huang M, Yan L, Zhang H, Shi C, Liu J, *et al.* Exosomes Derived from Baicalin-Pretreated Mesenchymal Stem Cells Alleviate Hepatocyte Ferroptosis after Acute Liver Injury via the Keap1-NRF2 Pathway. *Oxidative Medicine and Cellular Longevity*. 2022; 2022: 8287227. <https://doi.org/10.1155/2022/8287227>.
- [9] Chen X, Wang X, Hou Z. Editorial: MSC-derived exosomes in tissue regeneration. *Frontiers in Cell and Developmental Biology*. 2023; 11: 1293109. <https://doi.org/10.3389/fcell.2023.1293109>.
- [10] Maqsood M, Kang M, Wu X, Chen J, Teng L, Qiu L. Adult mesenchymal stem cells and their exosomes: Sources, characteristics, and application in regenerative medicine. *Life Sciences*. 2020; 256: 118002. <https://doi.org/10.1016/j.lfs.2020.118002>.
- [11] Hazan-Halevy I, Rosenblum D, Weinstein S, Bairey O, Raanani P, Peer D. Cell-specific uptake of mantle cell lymphoma-derived exosomes by malignant and non-malignant B-lymphocytes. *Cancer Letters*. 2015; 364: 59–69. <https://doi.org/10.1016/j.canlet.2015.04.026>.
- [12] Noack A, Gericke B, von Köckritz-Blickwede M, Menze A, Noack S, Gerhauser I, *et al.* Mechanism of drug extrusion by brain endothelial cells via lysosomal drug trapping and disposal by neutrophils. *Proceedings of the National Academy of Sciences of the United States of America*. 2018; 115: E9590–E9599. <https://doi.org/10.1073/pnas.1719642115>.
- [13] Zhang Y, Wang Y, Shao L, Pan X, Liang C, Liu B, *et al.* Knock-out of beta-2 microglobulin reduces stem cell-induced immune rejection and enhances ischaemic hindlimb repair via exosome/miR-24/Bim pathway. *Journal of Cellular and Molecular Medicine*. 2020; 24: 695–710. <https://doi.org/10.1111/jcmm.14778>.
- [14] Zhu L, Wang K, Cui J, Liu H, Bu X, Ma H, *et al.* Label-free quantitative detection of tumor-derived exosomes through surface plasmon resonance imaging. *Analytical Chemistry*. 2014; 86: 8857–8864. <https://doi.org/10.1021/ac5023056>.
- [15] Sun J, Shen H, Shao L, Teng X, Chen Y, Liu X, *et al.* HIF-1 $\alpha$  overexpression in mesenchymal stem cell-derived exosomes mediates cardioprotection in myocardial infarction by enhanced angiogenesis. *Stem Cell Research & Therapy*. 2020; 11: 373. <https://doi.org/10.1186/s13287-020-01881-7>.
- [16] Zhong L, Wang J, Wang P, Liu X, Liu P, Cheng X, *et al.* Neural stem cell-derived exosomes and regeneration: cell-free therapeutic strategies for traumatic brain injury. *Stem Cell Research & Therapy*. 2023; 14: 198. <https://doi.org/10.1186/s13287-023-03409-1>.
- [17] Lin HD, Fong CY, Biswas A, Bongso A. Hypoxic Wharton's Jelly Stem Cell Conditioned Medium Induces Immunogenic Cell Death in Lymphoma Cells. *Stem Cells International*. 2020; 2020: 4670948. <https://doi.org/10.1155/2020/4670948>.
- [18] Zhu L, Tian T, Wang J, He J, Chen T, Pan M, *et al.* Hypoxia-elicited mesenchymal stem cell-derived exosomes facilitates cardiac repair through miR-125b-mediated prevention of cell death in myocardial infarction. *Theranostics*. 2018; 8: 6163–6177. <https://doi.org/10.7150/thno.28021>.
- [19] Wang X, Jiao Y, Pan Y, Zhang L, Gong H, Qi Y, *et al.* Fetal Dermal Mesenchymal Stem Cell-Derived Exosomes Accelerate Cutaneous Wound Healing by Activating Notch Signaling. *Stem Cells International*. 2019; 2019: 2402916. <https://doi.org/10.1155/2019/2402916>.
- [20] Zhang L, Xiong Y, Yang Y. The Vital Roles of Mesenchymal Stem

- Cells and the Derived Extracellular Vesicles in Promoting Angiogenesis After Acute Myocardial Infarction. *Stem Cells and Development*. 2021; 30: 561–577. <https://doi.org/10.1089/scd.2021.0006>.
- [21] Yan D, Zhan S, Guo C, Han J, Zhan L, Zhou Q, *et al*. The role of myocardial regeneration, cardiomyocyte apoptosis in acute myocardial infarction: A review of current research trends and challenges. *Journal of Cardiology*. 2025; 85: 283–292. <https://doi.org/10.1016/j.jcc.2024.09.012>.
- [22] Kalluri R, Lebleu VS. The biology, function, and biomedical applications of exosomes. *Science*. 2020; 367: eaau6977. <https://doi.org/10.1126/science.aau6977>.
- [23] Cao L, Wang J, Zhang Y, Tian F, Wang C. Osteoprotective effects of flavonoids: Evidence from *in vivo* and *in vitro* studies. *Molecular Medicine Reports (Review)*. 2022; 25: 200. <https://doi.org/10.3892/mmr.2022.12716>.
- [24] Li X, Zhou X, Huang Z, Chen K, Jiang X, Lai R, *et al*. Study on the mechanism of naringin in promoting bone differentiation: *In vitro* and *in vivo* study. *Heliyon*. 2024; 10: e24906. <https://doi.org/10.1016/j.heliyon.2024.e24906>.
- [25] Gao C, Wu M, Du Q, Deng J, Shen J. Naringin Mediates Adult Hippocampal Neurogenesis for Antidepressant via Activating CREB Signaling. *Frontiers in Cell and Developmental Biology*. 2022; 10: 731831. <https://doi.org/10.3389/fcell.2022.731831>.
- [26] Li B, Mei X. Naringin may promote functional recovery following spinal cord injury by modulating microglial polarization through the PPAR- $\gamma$ /NF- $\kappa$ B signaling pathway. *Brain Research*. 2023; 1821: 148563. <https://doi.org/10.1016/j.brainres.2023.148563>.
- [27] Han X, Wang B, Sun Y, Huang J, Wang X, Ma W, *et al*. Metformin Modulates High Glucose-Incubated Human Umbilical Vein Endothelial Cells Proliferation and Apoptosis Through AMPK/CREB/BDNF Pathway. *Frontiers in Pharmacology*. 2018; 9: 1266. <https://doi.org/10.3389/fphar.2018.01266>.
- [28] Zhang Z, Hu P, Wang Z, Qiu X, Chen Y. BDNF promoted osteoblast migration and fracture healing by up-regulating integrin  $\beta$ 1 via TrkB-mediated ERK1/2 and AKT signalling. *Journal of Cellular and Molecular Medicine*. 2020; 24: 10792–10802. <https://doi.org/10.1111/jcmm.15704>.
- [29] Zhang L, Song L, Zhang P, Liu T, Zhou L, Yang G, *et al*. Solubilities of Naringin and Naringenin in Different Solvents and Dissociation Constants of Naringenin. *Journal of Chemical & Engineering Data*. 2015; 60: 932–940. <https://doi.org/10.1021/je501004g>.
- [30] Zhang H, Chen X, Xue P, Ma X, Li J, Zhang J. FN1 promotes chondrocyte differentiation and collagen production via TGF- $\beta$ /PI3K/Akt pathway in mice with femoral fracture. *Gene*. 2021; 769: 145253. <https://doi.org/10.1016/j.gene.2020.145253>.
- [31] Koch DW, Schnabel LV, Ellis IM, Bates RE, Berglund AK. TGF- $\beta$ 2 enhances expression of equine bone marrow-derived mesenchymal stem cell paracrine factors with known associations to tendon healing. *Stem Cell Research & Therapy*. 2022; 13: 477. <https://doi.org/10.1186/s13287-022-03172-9>.
- [32] Sharma A, Bhardwaj P, Arya SK. Naringin: A potential natural product in the field of biomedical applications. *Carbohydrate Polymer Technologies and Applications*. 2021; 2: 100068. <https://doi.org/10.1016/j.carpta.2021.100068>.
- [33] Bharti S, Rani N, Krishnamurthy B, Arya DS. Preclinical evidence for the pharmacological actions of naringin: a review. *Planta Medica*. 2014; 80: 437–451. <https://doi.org/10.1055/s-0034-1368351>.
- [34] Xu T, Luo Y, Wang J, Zhang N, Gu C, Li L, *et al*. Exosomal miRNA-128-3p from mesenchymal stem cells of aged rats regulates osteogenesis and bone fracture healing by targeting Smad5. *Journal of Nanobiotechnology*. 2020; 18: 47. <https://doi.org/10.1186/s12951-020-00601-w>.
- [35] Furuta T, Miyaki S, Ishitobi H, Ogura T, Kato Y, Kamei N, *et al*. Mesenchymal Stem Cell-Derived Exosomes Promote Fracture Healing in a Mouse Model. *Stem Cells Translational Medicine*. 2016; 5: 1620–1630. <https://doi.org/10.5966/sctm.2015-0285>.
- [36] Alva R, Gardner GL, Liang P, Stuart JA. Supraphysiological Oxygen Levels in Mammalian Cell Culture: Current State and Future Perspectives. *Cells*. 2022; 11: 3123. <https://doi.org/10.3390/ce111193123>.
- [37] Place TL, Domann FE, Case AJ. Limitations of oxygen delivery to cells in culture: An underappreciated problem in basic and translational research. *Free Radical Biology & Medicine*. 2017; 113: 311–322. <https://doi.org/10.1016/j.freeradbiomed.2017.10.003>.
- [38] Della Rocca Y, Fonticoli L, Rajan TS, Trubiani O, Caputi S, Diomedea F, *et al*. Hypoxia: molecular pathophysiological mechanisms in human diseases. *Journal of Physiology and Biochemistry*. 2022; 78: 739–752. <https://doi.org/10.1007/s13105-022-00912-6>.
- [39] Miceli V, Zito G, Bulati M, Gallo A, Busà R, Iannolo G, *et al*. Different priming strategies improve distinct therapeutic capabilities of mesenchymal stromal/stem cells: Potential implications for their clinical use. *World Journal of Stem Cells*. 2023; 15: 400–420. <https://doi.org/10.4252/wjsc.v15.i5.400>.
- [40] Toh WS, Lai RC, Hui JHP, Lim SK. MSC exosome as a cell-free MSC therapy for cartilage regeneration: Implications for osteoarthritis treatment. *Seminars in Cell & Developmental Biology*. 2017; 67: 56–64. <https://doi.org/10.1016/j.semcdb.2016.11.008>.
- [41] Wang Y, Chen W, Zhao L, Li Y, Liu Z, Gao H, *et al*. Obesity regulates miR-467/HoxA10 axis on osteogenic differentiation and fracture healing by BMSC-derived exosome LncRNA H19. *Journal of Cellular and Molecular Medicine*. 2021; 25: 1712–1724. <https://doi.org/10.1111/jcmm.16273>.
- [42] He L, Zhang H, Zhao N, Liao L. A novel approach in biomedical engineering: The use of polyvinyl alcohol hydrogel encapsulating human umbilical cord mesenchymal stem cell-derived exosomes for enhanced osteogenic differentiation and angiogenesis in bone regeneration. *International Journal of Biological Macromolecules*. 2024; 270: 132116. <https://doi.org/10.1016/j.ijbiomac.2024.132116>.
- [43] Eliceiri BP. Integrin and growth factor receptor crosstalk. *Circulation Research*. 2001; 89: 1104–1110. <https://doi.org/10.1161/hh2401.101084>.
- [44] Zhang Z, Zhang Y, Zhou Z, Shi H, Qiu X, Xiong J, *et al*. BDNF regulates the expression and secretion of VEGF from osteoblasts via the TrkB/ERK1/2 signaling pathway during fracture healing. *Molecular Medicine Reports*. 2017; 15: 1362–1367. <https://doi.org/10.3892/mmr.2017.6110>.
- [45] Bai L, Zhang S, Zhou X, Li Y, Bai J. Brain-derived neurotrophic factor induces thioredoxin-1 expression through TrkB/Akt/CREB pathway in SH-SY5Y cells. *Biochimie*. 2019; 160: 55–60. <https://doi.org/10.1016/j.biochi.2019.02.011>.
- [46] Zhang Z, Fan J, Ren Y, Zhou W, Yin G. The release of glutamate from cortical neurons regulated by BDNF via the TrkB/Src/PLC- $\gamma$ 1 pathway. *Journal of Cellular Biochemistry*. 2013; 114: 144–151. <https://doi.org/10.1002/jcb.24311>.
- [47] Huang S, Lin C, Lin H, Chiu C, Fang C, Liao K, *et al*. Brain-derived neurotrophic factor regulates cell motility in human colon cancer. *Endocrine-Related Cancer*. 2015; 22: 455–464. <https://doi.org/10.1530/ERC-15-0007>.
- [48] Matsuda S, Fujita T, Kajiyama M, Takeda K, Shiba H, Kawaguchi H, *et al*. Brain-derived neurotrophic factor induces migration of endothelial cells through a TrkB-ERK-integrin  $\alpha$ V $\beta$ 3-FAK cascade. *Journal of Cellular Physiology*. 2012; 227: 2123–2129. <https://doi.org/10.1002/jcp.22942>.
- [49] Lin C, Chen H, Li T, Fong Y, Liu S, Chen P, *et al*.  $\beta$ 5 integrin up-regulation in brain-derived neurotrophic factor promotes cell motility in human chondrosarcoma. *PLoS One*. 2013; 8: e67990. <https://doi.org/10.1371/journal.pone.0067990>.
- [50] Zhang B, Zhao J, Wang Z, Xu L, Liu A, Du G. DL0410 attenuates oxidative stress and neuroinflammation via BDNF/TrkB/ERK/CREB and Nrf2/HO-1 activation. *International Immunopharmacology*. 2020; 86: 106729. <https://doi.org/10.1016/j.intimp.2020.106729>.

**Editor's note:** The Scientific Editor responsible for this paper was Rui M. A. Domingues.

**Received:** 18th October 2024; **Accepted:** 9th January 2025; **Published:** 24th April 2025